CHAPTER 4

DIRECT FORCE MEASUREMENT

BETWEEN GOLD SURFACES IN XANTHATE SOLUTION

4.1 INTRODUCTION

4.1.1 Flotation and hydrophobicity

Froth flotation is a process, in which mineral particles with different hydrophobicity or hydrophilicity, are separated. Adhesion to air bubbles enables the hydrophobic particles to be recovered in froth stream, while the opposite go to the slurry stream. According to Yoon (91), the probability (P) of flotation can be evaluated by the following equation:

$$P = P_c P_a \left(1 - P_d\right) \qquad [1]$$

where P_c is the probability of bubble-particle collision, P_a is the probability of bubble-particle adhesion, and P_d is the detachment probability. Of these, P_c is strongly influenced by the hydrodynamic property of the flotation system, while P_a and P_d have intimate relationships with both the hydrodynamics and the surface forces between bubble and

particles (92, 93). Particles with higher hydrophobicity shows higher value of bubble-particle adhesion probability (P_a) and smaller detachment probability (P_d).

4.1.2 The theory to describe hydrophobicity: classic and extended DLVO theory

According to classical DLVO theory (94), the interaction surface energy between two macroscopic particles can be predicted by following relationship:

$$V_t = V_d + V_e \qquad [2]$$

where V_t is the total interaction energy, V_d represents the dispersion interaction energy, and V_e is the electrostatic interaction energy.

In the case of sphere-plate interaction, the London-van der Waals dispersion energy is given by:

$$V_d = -\frac{A_{132} R}{6H} \qquad [3]$$

where A_{132} is the Hamaker constant of between surface 1 and 2 in medium 3 (water), R is the radius of the sphere, and H represents the separation distance. We can transfer the energy function to force by integrating the above equation and obtain the following expression:

$$\frac{F_d}{R} = -\frac{A_{132}}{6H^2} \qquad [3b]$$

For electrostatic interaction energy which is due to the overlapping of the electrical double layers, we have Hogg, Feuerstenau and Henly's expression (95):

$$V_e = \frac{4\pi\varepsilon_0\varepsilon R_1 R_2\left(\Psi_1^{\,2} + \Psi_2^{\,2}\right)}{4(R_1 + R_2)}\left[\frac{2\Psi_1^{\,2}\,\Psi_2^{\,2}}{\Psi_1^2 + \Psi_2^2}\ln\left(\frac{1+e^{-\kappa H}}{1-e^{-\kappa H}}\right) + \ln\left(1-e^{-2\kappa H}\right)\right] \qquad [4]$$

here ε_0 and ε are the dielectric constant of water and the medium respectively, R_1, R_2 and Ψ_1, Ψ_2 are the radii and stern potential of the two interacting spheres respectively, and the κ is the reciprocal of the debye length. For the sphere-plate interactions, if the sphere and the surface are of the same material, we have

$R_{2(surface)} = \infty$, and $\Psi_1 = \Psi_2 = \Psi$

so the above expression [4] can be simplified to:

$$V_e = 4\pi\varepsilon_0\varepsilon R\Psi^2 \ln\left(1+e^{-\kappa H}\right) \qquad [5]$$

By integrating and normalizing the above equation, we have the electrostatic force given as:

$$\frac{F_e}{R} = 4\pi\varepsilon_0\varepsilon\kappa\Psi^2 \frac{e^{-\kappa H}}{1+e^{-\kappa H}} \qquad [5]$$

The classical DLVO theory, which only includes dispersion interaction force and electrostatic force but without considering structure force, has been applied to interpret the phenomena in many colloid systems during the past decades (96-100). However, the classical DLVO theory failed to explain the experimental results when the studied surfaces are strongly hydrated or covered with a hydrophobic surfactant such as in flotation system. It looks like there is a third force existed besides the commonly recognized van der Waals force and electrostatic force as in classic DLVO theory. With this consideration, Xu and Yoon (101,102) proposed the extended DLVO theory by including a third term (F_h) - which is referred as structure force - to the classical DLVO theory:

$$F_t = F_d + F_e + F_h \qquad [6]$$

Generally, all other forces except van der Waals force and electrostatic force, such as solvation, structural, hydration, hydrophobic, steric, fluctuation forces, etc., all can be attributed to the term of F_h (103). There are two empirical approaches in calculating the structure component currently. One of them is the double exponential function (104):

$$\frac{F_h}{R} = C_1 \exp\left(-\frac{H}{D_1}\right) + C_2 \exp\left(-\frac{H}{D_2}\right) \qquad [7]$$

where C_1, D_1, C_2, D_2 are constants, and H is the separation distance between the two approaching objects. If only the short range structure force existed, we can neglect the second term. The other approach is the power law (105):

$$\frac{F_h}{R} = \frac{K_h}{6H^2} \qquad [8]$$

where K_h is a constant.

As equation [7] has four parameters which is cumbersome to use while equation [8] has only one (K_h) which is comparable to the Hamaker constant directly, the second approach is more welcome to use.

Among the three force components in the extended DLVO theory, the first term (van der Waals force) can be calculated theoretically, second term (electrostatic force) is controlled by the electrolyte conditions in the system. Both do not have much direct relationship with adsorption of other molecules, such as surfactants, from the solution. On the other hand, the third term (structure force) is related directly with the solution environment, especially surface properties like reduction or oxidation, surfactants, etc. This information is of great importance to reveal the mechanism of surfactant adsorption and the stability of the system.

4.1.3 The direct force measurement techniques

Despite the utmost importance to get the information of the surface force for understanding the behavior of the colloid system, it is still very difficult to get the value of surface forces from theoretical calculation in most cases, mostly because there is no way yet to calculate theoretically the structure force component. Measuring the surface force directly is a practical way to fulfill this aim.

During the last 20 years, very important advances have been made in surface force measurement, partly due to the development of various techniques for measuring the distance dependence of these forces. These techniques include the surface force apparatus (SFA), MASIF (An instrument based on a bimorph force sensor), atomic force microscope (AFM), total internal reflection microscope (TIRM), and thin film balance (TFB), etc (106). Among these techniques, Surface Force Apparatus (SFA) and Atomic Force Microscope (AFM) are the most widely used in studying the adsorption mechanism and the interaction in particle/surfactant systems by applying the extended DLVO theory.

4.1.3.1 Surface Force Apparatus (SFA)

Developed by Isrealachvili and Adams (107), SFA is the most commonly used method to measure the force between two solid surfaces in liquid medium. A schematic drawing of the apparatus is shown in Figure 4.1. The force measurement is conducted between two curved surfaces (usually mica) offset by 90^0, i.e., crossed-cylinder geometry, where one is mounted on a piezo-electric crystal and the other on a weak spring. White

light is directed through the surfaces, and fringes are produced which are used to monitor the separation distance between the surfaces with an accuracy of 0.1 nm. The observed forces are calculated from the deflection of the spring as the surfaces approach each other.

Over the last two decades, a wealth of information on the structure of interfaces and the nature of intermolecular forces has been amassed by use of direct force measurements with surface force apparatus (SFA) (108-113). A primary limitation of this instrument is the need for molecularly smooth and optically transparent surfaces to obtain accurate force data. For this reason most studies have been limited to mica (108-111) or coating the object material on the surface of mica (112, 113). The technique is useful to understand the mica system, however, because most minerals are non-transparent, it can not be used to study the general systems, such as sulfide flotation.

4.1.3.2 Atomic Force Microscope (AFM)

The advent of the atomic force microscope (AFM) in 1985 (114) has made possible the study of a much broader range of materials. Using a reflective laser beam to measure the relative position of the surface distances, this technique does not require transparent a prerequisite for the material to be studied. A schematic drawing of the apparatus is also

Fig. 4.1 Schematic drawing of SFA and AFM (115)

shown in Figure 4.1. As shown in the figure, the AFM measures the surface force by moving the flat sample which is mounted on the top of a piezo-electric tube toward the cantilever with the help of a step motor, while monitoring the deflection of the cantilever by using of laser light beam and a diode detector. As the deflection of the cantilever is caused by the attraction or dispersion interaction between the studied surface and cantilever, its values can be transformed to the surface force. The approach of using the deflective light to measure the interaction between surfaces allows direct force measurement with a great number of materials which are not optically transparent. However, as the technique studies the force between two objects at the molecular level, the smoothness of the surfaces is obviously of critical importance. Only the materials with surfaces of molecular smoothness can be studied accurately by AFM. Many studies are conducted on materials with the natural smooth crystal structure, such as mica (116, 117), graphite (118), silica (115, 119), and covelite (120). The surface force between the surfaces of other materials besides mica, silica, etc., such as titanium oxide (121, 122), polypropylene (123), gold (124, 125), zirconia (126), and zinc sulfides (127), alumina (128) and etc., also have been studied recently. However, the probe and/or surface they used were pretty rough (see Fig. 4.2). The problem with a rough surface is that even when an unambiguous zero of separation can be determined from a force curve, the question still needs to be posed as to exactly what is “contact” for two rough surfaces. It undoubtedly results in errors during the measurements and brings difficulties in interpreting the results.

4.1.4 Surface force study with gold

Gold is one of the most chemically inert metals, and can not be attacked by water or air (129). It plays an important role in colloid chemistry. Faraday's gold gel, prepared by the reduction of gold (III) chloride with citrate anions in aqueous solution, is one of the earliest and most well documented examples of the preparation of a stable colloid in the laboratory (125). Although many of the studies have been conducted using various electrochemical and spectroscopic techniques (130-133), the role of each anion in determining the stability of both the nascent and final gold particles has not been clearly established. On the other hand, as a mineral, its interaction with xanthate has been regarded as a model for consideration of the electrochemical aspects of the flotation of sulfide minerals (134). It is meaningful to study the gold systems for a better understanding of gold colloid stability and the electrochemical mechanism of sulfide flotation.

The advent of the AFM technique makes it possible to study the colloid systems directly. Biggs et al. (125) studied the anion adsorption on gold surface using AFM in the presence of various electrolytes, such as gold chloride, sodium chloride, and trosodium citrate, etc. From direct surface force measurements, they revealed that in addition to electrostatic repulsive forces, unexplained short range repulsions are present at the gold/water interface in the presence of adsorbed anions. It is the presence of this short range surface force in citrate solutions that prevents gold colloid coagulation.

Fig. 4.2. Rough surfaces used in some AFM studies (122, 125)

The surface force between a flat gold surface and a gold coated silica sphere in water was also studied using AFM technique by Biggs and Mulvaney (135). They measured a very strong van der Waals interaction between gold surfaces in water. After fitting the measured force curves with DLVO theory, they got a value of $2.5 \pm 0.5 \times 10^{-19}$ J for the unretarded Hamaker constant for gold in water.

However, despite some information about gold colloid stability and surface properties in aqueous medium that were revealed by above studies, due to the difficulty in obtaining molecularly smooth gold surface as mentioned above, there is no research reported to date yet which shows a force curve with enough accuracy to be resolved by extended DLVO theory to depict more detailed information such as the hydrophobic force, hydration force, and etc.

4.1.5 The objective of the investigation

By measuring the surface force between gold surfaces in xanthate solution using AFM technique, the present research tries to reveal the mechanism of xanthate adsorption on gold surface, and figure out what xanthate species in gold-xanthate system is responsible for the gold surface hydrophobicity. Gold-xanthate system is selected because 1) it is possible to get the optically smooth surface of gold (129); (2) it is very stable in aqueous solutions; and (3) xanthate is a widely used collector in sulfide flotation.

4.2 EXPERIMENTAL

4.2.1 Gold sphere and surface:

The gold spheres were made by melting the gold powders with the size of around 2 to 3 micron which was obtained from Alfa Products, MA. The gold powders are melted by placing them in a furnace with the temperature at about 1100 °C. The furnace was flushed with nitrogen to maintain oxygen-free atmosphere. Some fine particles are melt together forming bigger gold spheres after the melting. The material was cooled down to room temperature. By this way, gold spheres with size range from several microns to about 100 micron were made. Among these, only the spheres in a size range of 20 to 40 micron were selected for experiments.

Fig. 4.3 is a SME picture of a gold sphere used in the present investigation. The gold surface was prepared by sputtering gold directly onto the surface of an optically smooth silica plate. The gold-sputted surface was checked by examining the AFM images before force measurement to make sure that it is of molecular smoothness. The image of the surface shows that the surface has an average surface roughness of less than 5 nm and is considered to be smooth enough for present investigation.

Fig. 4.3 Photo of gold sphere used in the present investigation

4.2.2 Reagents:

Potassium ethyl xanthate (KEX) and potassium amyl xanthate (KAX) were used in the experiments. The reagent grade xanthate was recrystallized from acetone three times prior to use. Sodium borate was used as the supporting electrolyte which produced a naturally buffered pH of 9.2 at the concentration of 0.03M. Solutions were made using 18-m ohm deionized water.

4.2.3 AFM apparatus and force measurements

A Naroscope III atomic force microscope developed by Digital Instruments was used to measure the surface forces between the gold surfaces prepared. The AFM equipped with a standard liquid cell was shown schematically in Fig. 4.4. A gold sphere of 20-40 μm diameter was attached to the end of an AFM cantilever (b) using an epoxy resin, which has found not to contaminate the aqueous liquid medium (135). The sphere and cantilever were placed in an AFM liquid cell (c) with an O-ring (d) between the cell and the gold surface (e) to form a water-tight cavity. The water medium was injected into the cavity (f) through one of the two liquid ports (g) by means of a syringe. Monochromatic light emitted from a laser diode (h) was reflected off the cantilever to a split photodetector (i) to monitor the position of the sphere. As the piezoelectric scanner (j) moved the gold surface to the sphere probe, the cantilever was deflected from its original position depending on the nature of the surface forces acting between the gold sphere and gold surfaces.

Fig. 4.4 AFM apparatus with liquid cell (115)

Before measuring the surface forces between the gold sphere and the gold plate, the liquid with desired xanthate concentration was injected to the cell. Precautions was taken to prevent introducing air bubble to the cell. By recording the relative position of the sphere and the surface with a reflective laser beam, a deflection vs. Z (sample displacement in z direction) curves was obtained by moving the gold surface mounted on a piezoelectric crystal along the z direction toward the gold sphere which is glued to the cantilever while monitoring the cantilever deflection. The actual force vs. separation distance plots were obtained by using appropriate values for the spring constant of the cantilever and the radius of sphere glued to the cantilever.

4.2.4 Contact angle measurements:

Contact angles were measured using a Rame-Hart Model 100 goniometer by depositing a nitrogen bubble on the gold surface in the solution with desired xanthate concentration. The gold surface is polished with alumina powder and rinsed with double distilled water before each measurement. At least 10 measurements were made to get the averaged value of the contact angle for each case.

4.2.5 FTIR measurements:

Fourier Transform Infrared (FTIR) spectroscopic measurements were conducted on gold plate under different xanthate concentration using external reflection technique. A total of 64 scans were recorded at 4 cm^{-1} resolution using a Bio-Rad FTS 60A FTIR spectrometer. The gold plate was immersed in the solution with desired xanthate

concentration for 5 minutes and then was put into the sample cell of FTIR and recorded the spectrum immediately. Between each measurement, the gold plate was polished with alumina powder and rinsed by distilled water completely. A background spectrum of the plate was also collected and subtracted from the adsorption spectra. The different spectra were then baseline-collected prior to analysis.

4.3 RESULT

4.3.1 Contact angle measurements

Fig. 4.5 shows the measurements of the contact angle established for gold surface in a pH 9.2 buffer solution under different KEX and KAX concentration. It can be seen that, in ethyl xanthate solution, the gold surface remains hydrophilic at lower xanthate concentration. When the concentration was increased over a critical point around 8×10^{-3} M, the measured contact angle increased significantly and reached a maximum of about 66 degrees at the concentration of 5×10^{-2} M. For amyl xanthate, there is also a critical concentration (5×10^{-4} M) existing between the hydrophilic and hydrophobic phase. Comparing with ethyl xanthate, this critical concentration is lesser by an order of magnitude. It shows that xanthate demonstrates a much stronger hydrophobizing power with a longer hydrocarbon chain.

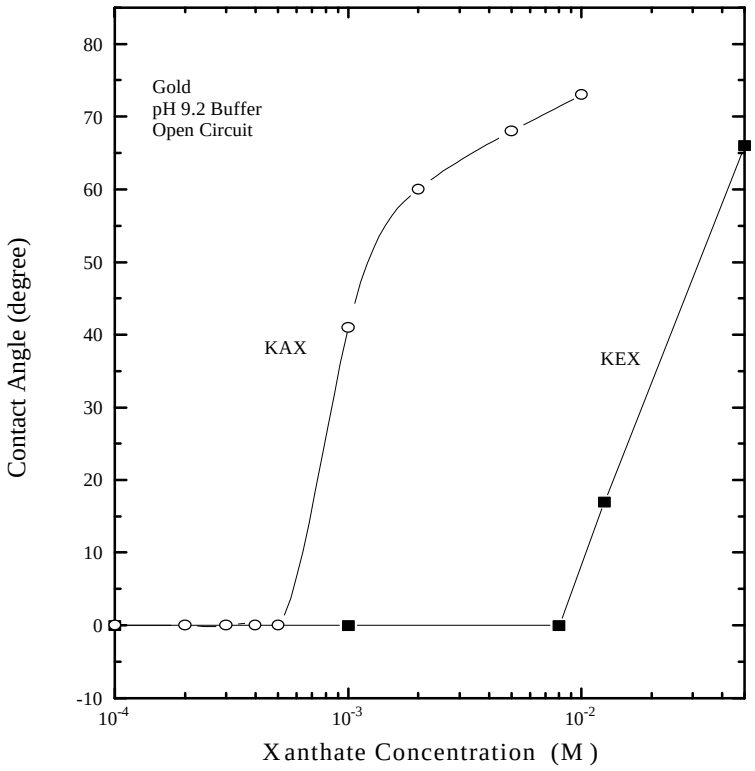

Fig.4.5 Contact angle measurements in KEX and KAX at pH 9.2 with different xanthate concentrations

4.3.2 Surface force measurements using AFM

4.3.2.1 Measurements between sphere and surface without xanthate in solution

Fig. 4.6 shows the forces measured between gold sphere and gold plate in a pH 9.2 buffer solution without any xanthate. The solid circles represent the experimental data, while the solid and dashed lines represent the classic DLVO theory and extended DLVO theory, respectively. It shows that when the separation distance between the sphere and surface is larger than 16 nm, no interaction force is observed. At shorter separation distance, the interaction force becomes strongly dispersive. No hydrophobic force is observed.

Although the classical DLVO theory fits the measured force curve very well, the discrepancy between the experimental data and the theory become more and more significant, as the sphere and plate get closer to each other. As the classic DLVO theory considers only two component, i.e., van der Waals force and electrostatic force in the system, this discrepancy may come from another force which exists only in short range. Since no surfactant but electrolyte (i.e., sodium phosphate, used for making buffer solution) was added to the system, this extra force component may be a hydration force. With this consideration, the experimental data were fitted to the extended DLVO theory, by including a third force component, hydration force, into the classical DLVO theory. The new theory fits the experimental data very well. Exponential force law

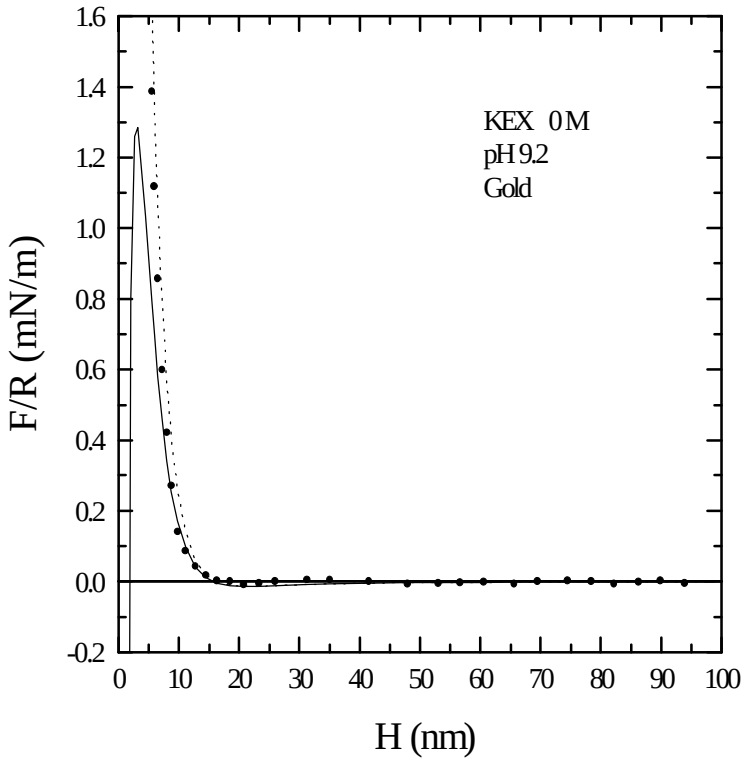

Fig.4.6 Surface force measurements in pH 9.2 buffer solution

with the second term omitted was used to fit the hydration force. The fitting results shows that the gold-water system in the pH 9.2 buffer solution has a Hamaker constant of 4.8 x 10^{-20} J, surface potential of -52 mv and a debye length of 2.82 nm. The fitted surface potential (-52 mv) shows a very good agreement with the data calculated from nonlinear Poisson-Botzmann equation (as shown in Fig. 4.7). The fitted short decay length (D_1) and the exponential constant (C_1) for the hydration force are 1.9 nm and 15 mN/m, respectively.

There is a great deal of discrepancy against the values of the Hamaker constants for gold in aqueous medium in literature. Enustun and Turkevich (130) reported a value of 2.3 x 10^{-20} J from the study of coagulation of colloidal gold. Reerink and Overbeek (136) also got the value in the range of (0.5-1) x 10^{-20} J to 6 x 10^{-20} J. However, from theoretical calculation and AFM force measurement, Biggs et. al. (125, 135) got a Hamaker constant for gold surfaces in water to be ten times higher than the value from Enustun and Reerink's work. Israelachvili showed that gold possesses a Hamaker constant value of (3-5) x 10^{-19} J in water in his book (103). However, the same book also shows that the Hamaker constant of gold in vacuum is the same value as in water medium (103). This makes things confusing. According to Israelachvili (103), the Hamaker constant of a material in aqueous medium should be lower than that in vacuum medium, and there is a relationship shown bellow:

$$A_{gold-water} = \left(\sqrt{A_{gold-air}} - \sqrt{A_{water-air}}\right)^2 \qquad (9)$$

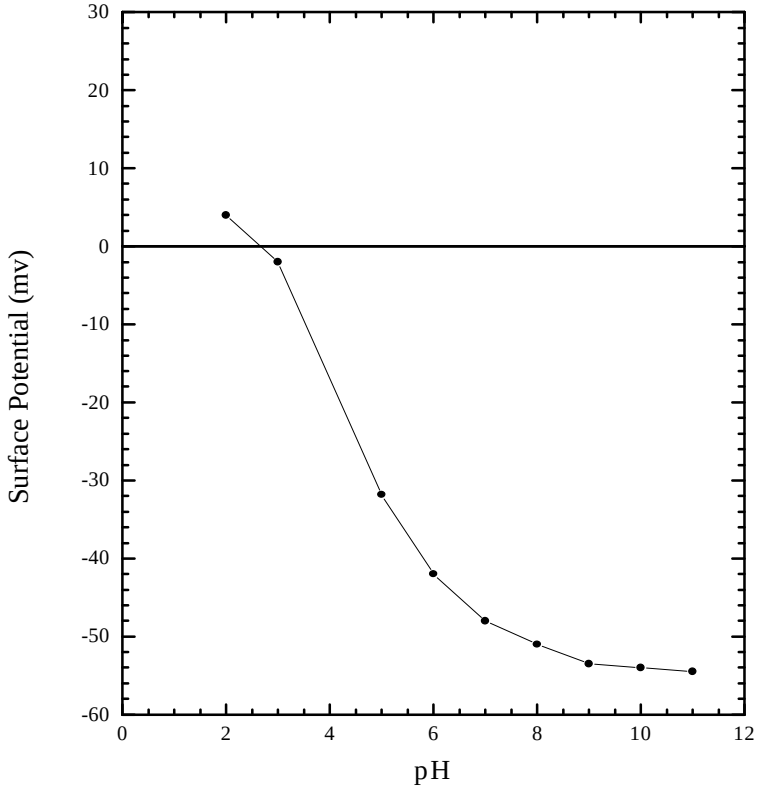

Fig. 4.7 The relationship between gold surface potential and solution pH

According to Israelachvili (103), the values of $A_{gold\text{-}air}$ and $A_{water\text{-}air}$ were (2.5-4) x 10^{-19} J and 4.0 x 10^{-20} J, respectively. Substitute these values into the Equation (9), we get the value of the Hamaker constant for the gold in water to be about 1 to 10 x 10^{-20} J. Our value for gold Hamaker constant in water was fitted to be 4.8 x 10^{-20} J, which agrees well with the above calculation and Enustun's results (130).

4.3.2.2 Surface force measurements in ethyl xanthate solution

The result of the measured force between gold sphere and surface in the 1 x 10^{-2} M ethyl xanthate (pH 9.2 buffer) solution is shown in Fig. 4.8. Similar to the case in pure buffer solution, it shows that there is no surface force observed between the studied gold sphere and surface when the distance is large. Only when the separation distance is less than 15 nm a strong dispersion force emerged. No hydrophobic force is observed either. The fitted parameters, i.e., Hamaker constant, surface potential and debye length, of the experimental data are the same as the former case (as shown in Fig. 4.3), except the short decay length (D_1) of 2.0 nm and the strength (C_1) of 10 mN/m for the fitted hydration force component.

When the concentration of ethyl xanthate increases to 2 x 10^{-2} M, the gold surface becomes hydrophobic with the gold sphere jumping to the gold surface when the latter approaches the former close enough. As shown in Fig. 4.9, the force curve shows a jump at the separation distance of about 33 nm. The force curve was fitted to the extended DLVO theory which includes a hydrophobic force component besides van der Waals force and electrostatic force components. The fitted van der Waals force and electrostatic force

are calculated using the above fitted Hamaker constant, surface potential and debye length. The hydrophobic force was represented by the power law with a hydrophobic constant of 2.22 x 10^{-19} J. This hydrophobic constant is about four times as large as the Hamaker constant (4.8 x 10^{-20} J).

As the ethyl xanthate concentration is further increased to 5×10^{-2} M, the hydrophobic force component in the total force became even stronger (Fig. 4.10). The jumping distance increased to about 45 nm from 33 nm in the above case and the hydrophobic constant increased to 6.66×10^{-19} J, which is about eleven times bigger than the value of the Hamaker constant. This suggests a much stronger hydrophobic force between the sphere and plate.

4.3.2.3 Surface force measurements in amyl xanthate solution

Fig. 4.11 shows the measured surface force between the gold sphere and surface in 1 x 10^{-3} M amyl xanthate solutions. It shows a much stronger hydrophobic attraction than the former cases with ethyl xanthate. The curve was fitted with a hydrophobic force constant of 186×10^{-20} J, which means the hydrophobic force is about seven times as strong as the van der Waals dispersion force in the case. When the concentration of amyl xanthate is 2.5×10^{-3} M (as shown in Fig. 4.12), the gold surface is more

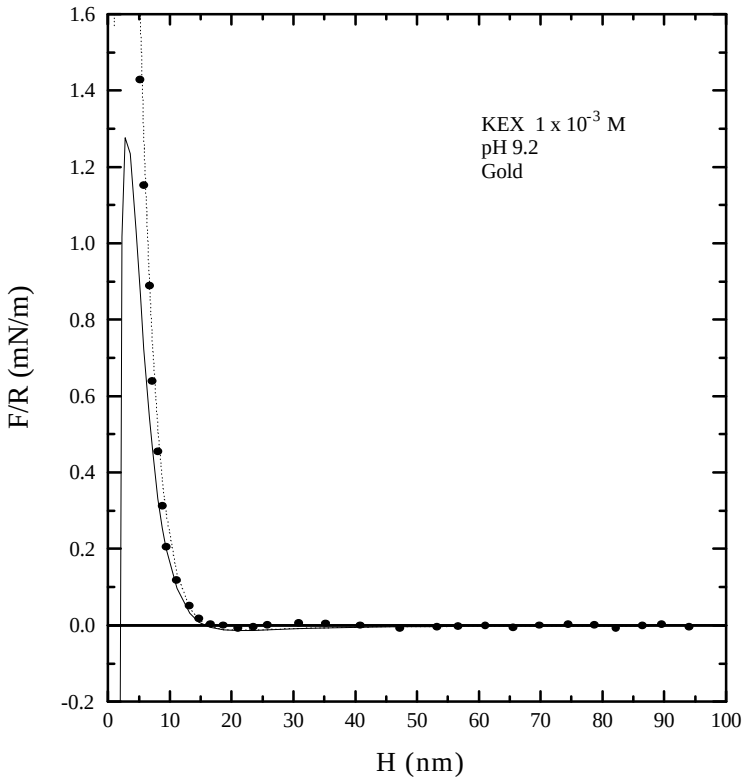

Fig. 4.8 Surface force measurements in the buffer solution with 1×10^{-2} M KEX

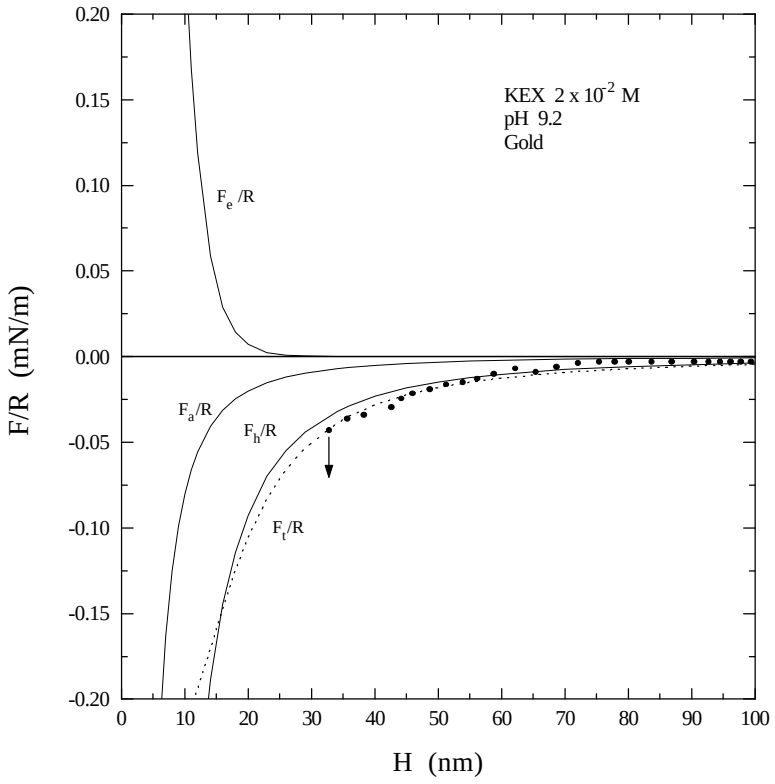

Fig. 4.9 Surface force measurements in the buffer solution with 2×10^{-2} M KEX

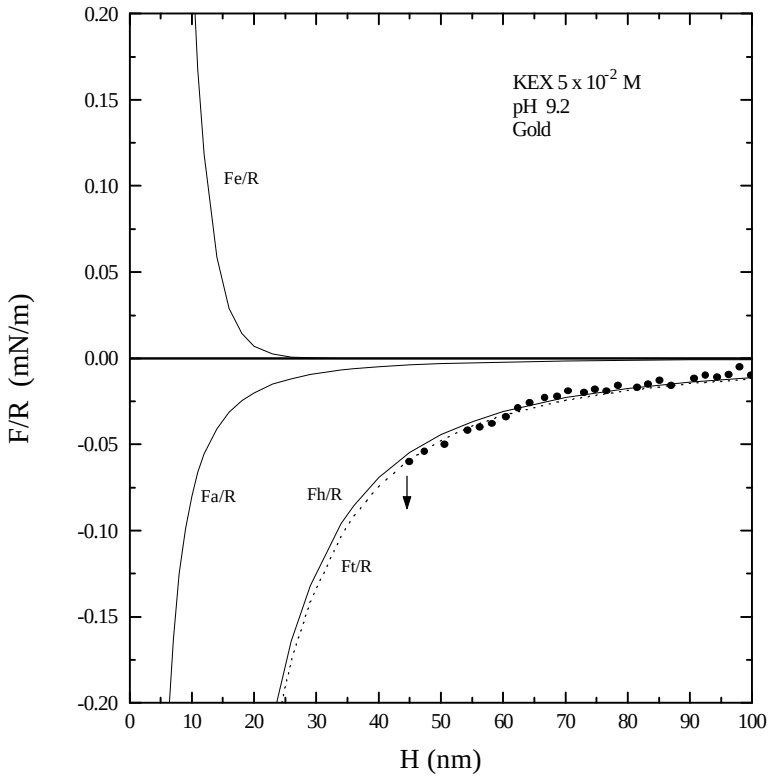

Fig. 4.10 Surface force measurements in the buffer solution with 5×10^{-2} M KEX

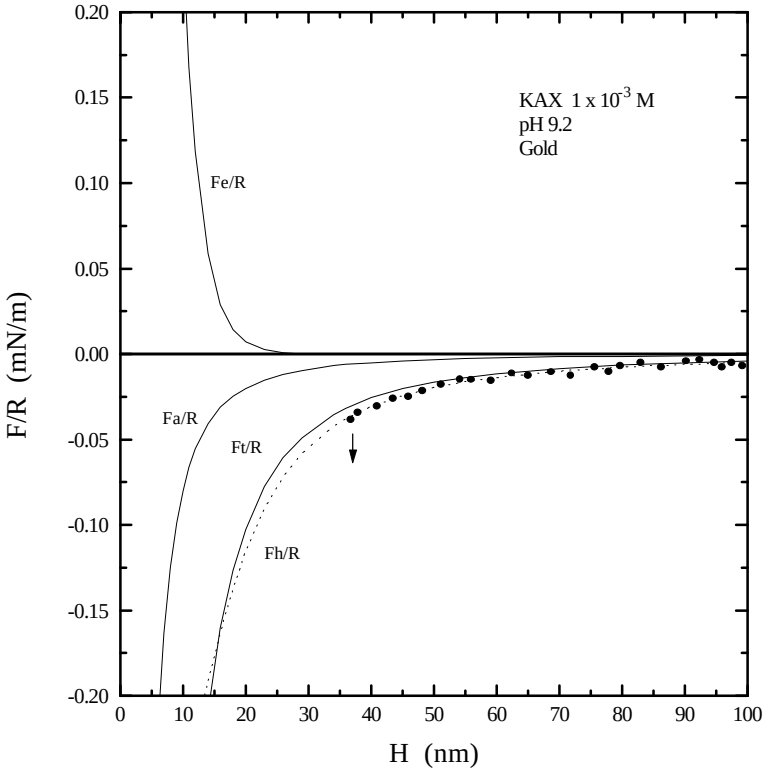

Fig. 4.11 Surface force measurements in the buffer solution with 1×10^{-3} M KAX

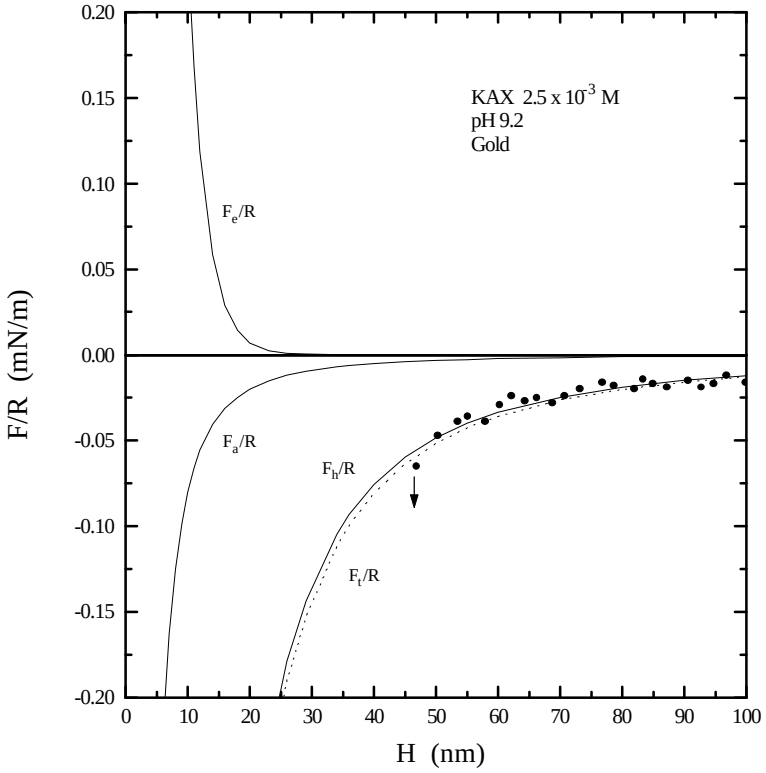

Fig. 4.12 Surface force measurements in the buffer solution with 2.5×10^{-3} M KAX

hydrophobic with a jumping distance of nearly 50 nm and hydrophobic constant of 310×10^{-20} J.

The above results reveal that the gold surface is more hydrophobic in amyl xanthate solution than in ethyl xanthate solution. While it is still hydrophilic at the concentration of 7×10^{-3} M with ethyl xanthate, the gold surface is strongly hydrophobic in 1×10^{-3} M amyl xanthate solution. This is consistent with the contact angle measurements. When the xanthate concentration is low or zero (pure buffer solution), corresponding a zero contact angle, the measured force curve is repulsive and no hydrophobic force is observed, which means the surface is hydrophilic. When the xanthate concentration gets higher, a positive contact angle on gold surface is observed, and the force curves show a jump which means the surface and sphere sticks together due to hydrophobic force. Further increasing the xanthate concentration renders the gold surface more hydrophobic, presented a larger contact angle, a larger jumping distance and a more significant hydrophobic force component in the force curves.

4.4 DISCUSSION

According to Yoon (137), xanthate adsorbs on conductive minerals (such as sulfide, gold, etc.) through one of the following three reactions or the combination of them:

(a). Chemisorption of the thiol ion (X^-):

$$X^- \rightarrow X_{ads} + e \qquad [10]$$

(b). the oxidation of the thiol ion to the corresponding dithiolate:

$$2\ X^- \rightarrow X_2 + 2e \qquad [11]$$

(c). the reaction of thiol with the mineral to form a metal xanthate compound, such as:

$$2\ X^- + M^{++} \rightarrow MX_2 + 2e \qquad [12]$$

In above reactions, X^- stands for the xanthate ion. M and M^{++} stand for metal atom and ion, respectively. All the above three reactions are electrochemical reactions, which involve electron transfer, coupled with a cathodic reaction such as the reduction of oxygen,

$$O_2 + 2H_2O + 4e \rightarrow 4OH^- \qquad [13]$$

From the gold Eh-pH diagram as shown in Fig. 4.13, we can see that gold is very stable and can not be oxidized in the solution in the pH range from 1 to 10 when the potential is below 1 v (SHE). So we can assume that, in the present investigation, which

is conducted at pH 9.2 and open circuit, gold is stable in aqueous environment and there is hardly any appreciable amount of gold ions dissolved in the solution. In other words, among the three possible xanthate-gold reactions, only the reactions (a) and (b) may be possible.

Fig. 4.14 is the FTIR spectra of gold in the pH 9.2 buffer solutions with different concentrations of ethyl xanthate in it. From the referent spectra for gold xanthate and dixanthogen as shown in Fig. 4.15, we can see that gold xanthate has identical peaks at 1121 cm^{-1} and 1196 cm^{-1} and dithanthogen at 1269 cm^{-1} and 1107 cm^{-1}. Due to the difficulty in isolating samples of xanthate, the characteristic peaks of chemisorbed xanthate on gold have been calculated to be 1204 cm^{-1} by Ihs et al. (138) from the value of gold xanthate. It can be seen from Fig. 4.14 that only chemisorbed adsorbance peak at 1204 cm^{-1} is observed when the concentration of ethyl xanthate is lower than 1 x 10^{-3} M. At higher ethyl xanthate concentrations, dixanthogen adsorption is also observed besides the chemisorption, and the dixanthogen adsorption intensity is increased with the increase of the xanthate concentration in the solution.

Comparing the infrared spectra, value of contact angle, the fitting parameters for structure force component all together in Table 4.1, we can see more clearly the relationship among xanthate concentration, contact angle, and the hydrophobicity in gold-xanthate system. While xanthate chemiadsorbs on the gold surface with almost the same intensity for xanthate concentration from 1×10^{-3} M to

Fig. 4.13 Eh-pH diagram of gold (129)

Fig. 4.14. FTIR spectra of gold after xanthate adsorption

Fig. 4.15. The reference spectra of gold xanthate and dithanthogen

5×10^{-2} M, dixanthogen species is observed only at higher amyl xanthate concentration (higher than 1×10^{-2} M), and its intensity increases with the increase of xanthate concentration. Although there is chemisorption observed on the gold surface in xanthate solution, the surface remains hydrophilic with low contact angle and zero hydrophobic constant until dixanthogen is formed when the ethyl xanthate concentration is higher than 1×10^{-2} M. There is a very good correlation between dixanthogen forming and the hydrophobicity of the gold surface. It can be concluded that the dixanthogen is only species in the system that contribute to the hydrophobicity of gold surface. Amyl xanthate has a lower oxidation potential (-0.157 v) than ethyl xanthate (-0.057 v) (137), which means that it is easier than the latter to be oxidized to form dixanthogen in solution or on the surface of gold through equation [11]. As the dixanthogen is the hydrophobic species in gold-xanthate system, amyl xanthate is more powerful to render the gold surface hydrophobic than ethyl xanthate.

Table 4.1 The properties of gold surface under different xanthate concentrations

Collector	Conc. (M)	Contact Angle	Jump Dist.	K_h (x 10^{-19} J)	X_{ads}* Intensity	X_2** Intensity
KEX	1×10^{-3}	0	--	0	0.0009	0
	1×10^{-2}	8	--	0	0.0009	0
	2×10^{-2}	34	33 nm	2.2	0.0010	0.0017
	5×10^{-2}	67	45 nm	6.7	0.0010	0.0029
KAX	1×10^{-3}	42	37 nm	2.5		
	2.5×10^{-3}	62	47 nm	7.3		

* at 1204 cm^{-1}
** at 1269 cm^{-1}
$A_{121} = 4.8\times10^{-20}$ J

CHAPTER 5

SUMMARY AND CONCLUSIONS

1. Atomic force microscope (AFM) has been used successfully to study the xanthate adsorption on the gold surface.
2. At lower xanthate concentration, the surface of gold remains hydrophilic with zero contact angles and no observation of hydrophobic force.
3. At higher xanthate concentrations, dixanthogen species is formed on the surface. For ethyl and amyl xanthate, the critical concentration are 8×10^{-3} M and 5×10^{-4} M, respectively. With further increase in the xanthate concentration, the contact angle is increased significantly and significant hydrophobic forces are observed.
4. Contact angle and surface force measurements showed that amyl xanthate is more powerful in rendering gold surfaces hydrophobic.
5. Classical DLVO theory can be used to explain the measured force when no structure forces are present. When the surface is strongly hydrophilic or hydrophobic, classical DLVO theory can not be used to explain the results.
6. Extended DLVO theory, which includes a third force - structure force - besides the van der Waals force and electrostatic force, can be used to interpret the experimental results. The structure force can be fitted by exponential law or power law.
7. The fitting results with extended DLVO theory yielded that gold has a Hamaker constant of 4.8×10^{-20} J, surface potential of -52 mv, and debye length of 2.82 nm in

the aqueous medium of pH 9.2 buffer solution. When the gold surface is hydrophobic, the fitted hydrophobic force is about 10 times stronger than van der Waals force.

8. In the xanthate-gold system, only dixanthogen contributes to rendering the gold surface hydrophobic. Chemisorbed xanthate specie is observed on the gold surface but it is hydrophilic.
9. The surface of coal pyrite is usually oxidized and can be floated without collector.
10. Non-polar kerosene improves coal pyrite floatability, so deteriorates coal-pyrite separation selectivity.
11. Among the 11 polymeric depressants tested, depressants 17580-101, 17305-185, and S-7261 are capable of improving the rejection of sulfur, specifically pyritic sulfur, in the flotation of Pittsburgh No. 8 coal.
12. At a reagent dosage of 100 g/t, these reagents can depress coal pyrite in Pittsburgh No. 8 coal sample without significantly affecting the flotation kinetics of coal. However, at reagent dosages greater than 300 g/t, the flotation kinetics of coal is reduced significantly
13. The depression effect of polymers on Illinois No. 6 coal sample is not as effective as for Pittsburgh No. 8 coal sample.
14. When using S-7261, the reagent dosage should be limited to below 300 g/t for both Pittsburgh No. 8 and Illinois No. 6 coal samples. The optimum dosage is near 150 g/t for both coal samples. At higher dosages, depression of the coal is observed.

15. The nickeliferous pyrrhotite in the pentlandite ore tested in the present work tends to float without a collector, which may be a cause for the difficulty in removing pyrrhotite by flotation.
16. In the presence of the thiol collectors tested in the present work, pyrrhotite rejection improves significantly, indicating that the collectors adsorb on pentlandite in preference to pyrrhotite and help the former float faster than the latter.
17. The polymeric depressant S-7261 shows comparable pyrrhotite depression effect as DETA. The polymeric depressants can depress pyrrhotite effectively with relatively small sacrifice of pentlandite recovery. Polymer S-7260 also shows some prospect.
18. The dosage of xanthate plays an important role in the selective separation of pentlandite with pyrrhotite. When the xanthate dosage is higher than 250 g/t, the collector floats both pentlandite and pyrrhotite non-selectively. When the xanthate dosage is lower than 100 g/t, the floatability of both pentlandite and pyrrhotite are low, and no selective flotation emerged even depressant added, not recommended. The optimum xanthate dosage should between 150 to 250 g/t.

CHAPTER 6

FUTURE WORKS

On the bases of the research that has been conducted during this investigation, the following areas for future research are suggested:

1. A study should be carried out to delineate the adsorption mechanism of polymers on the surface of coal and pyrite. This can be achieved by conducting measurements of FTIR spectra under different conditions.
2. Experiments on pilot and/or plant scale should be conducted to verify the effect of the polymers, especially 17580-101, 17305-185 and S-7261, which show significant improvement in laboratory tests.
3. An effort should be made to study the effect of particle size on the flotation performance of pentlandite and pyrrhotite and as well as their liberation behavior.
4. More flotation tests of polymeric depressant S-7260 on pyrrhotite depression.
5. Spectroscopic measurements to reveal the depression mechanism of the polymeric depressants, especially S-7261.
6. Industrial scale tests on the depression effect of the polymers on pentlandite flotation.
7. Using AFM, measure the surface force on gold surface without buffer solution.
8. A series of tests should be conducted to measure the surface force on gold surface under different pH, xanthate concentration and applying potential to the system.
9. Using AFM technique, study the interaction of hydrocarbon chains between the molecules of xanthate and polymers.